Saudi Journal of Biological Sciences 27 (2020) 1130–1138

Contents lists available at ScienceDirect

Saudi Journal of Biological Sciences

journal homepage: www.sciencedirect.com

Original article

Novel synthesis of ZnO by Ice-cube method for photo-inactivation of *E. coli*

Perumal Dhandapani [a,b], Sandhanasamy Devanesan [c,d], Jayaraman Narenkumar [e], Sundaram Maruthamuthu [a], Mohamad S. AlSalhi [c,d,*], Aruliah Rajasekar [b,*], Anis Ahamed [f]

[a] *Corrosion and Material Protection Division, CSIR-Central Electrochemical Research Institute, Karaikudi 630006, India*
[b] *Environmental Molecular Microbiology Research Laboratory, Department of Biotechnology, Thiruvalluvar University, Serkkadu, Vellore 632115, Tamil Nadu, India*
[c] *Research Chair in Laser Diagnosis of Cancers, Department of Physics and Astronomy, College of Science, King Saud University, Riyadh, Saudi Arabia*
[d] *Department of Physics and Astronomy, College of Science, King Saud University, P.O. Box 2455, Riyadh 11451, Saudi Arabia*
[e] *Shenyang National Laboratory for Materials Science, Northeastern University, Shenyang 110819, China*
[f] *Department of Botany and Microbiology, College of Science, King Saud University, P.O. Box 2455, Riyadh 11451, Saudi Arabia*

ARTICLE INFO

Article history:
Received 26 December 2019
Revised 21 January 2020
Accepted 1 February 2020
Available online 11 February 2020

Keywords:
Ice-cube
XRD
E. coli
Antibacterial activity
AFM

ABSTRACT

The ZnO particle with varieties of morphology was prepared from ice-cube of zinc ammonium complex at boiling water surface in 1 min induction of thermal shock. The zinc ammonium complex in ice cube was developed using zinc acetate and biologically activated ammonia in 1 hr and kept in the freezer. Temperature gradient behaviour of the water medium during thermal shock was captured by the thermal camera and thermometer. Morphology study revealed a variety of flower-like ZnO particles with variable size from 1.0 to 2.5 μm. Further, ZnO particle morphologies were tuned by adding trisodium citrate and hexamine to obtain uniform spherical (2–3 μm) and flower (3–4 μm) shapes, respectively. XRD patterns revealed that all ZnO samples are of a hexagonal structure. Photocatalytic inactivation of *E. coli* has been investigated using various particle morphologies of ZnO in an aqueous solution/overcoated glass slide under sunlight. The photo-inactivation of *E. coli* by ZnO particles in suspension condition was better when compared to a coated glass slide method. AFM study confirmed the destruction of bacterial cell wall membrane by the photocatalytic effect. The particles morphology of photocatalyst is well dependent on antibacterial activity under sunlight.

1. Introduction

Fabrication of nano-to microscopic-scale inorganic materials with unique morphology is of enormous interest for materials science because of its importance in basic scientific research and potential technological applications (Zhou et al., 2015). The shape, crystalline structure, and size of Zinc oxide (ZnO) particles are determining their physical and chemical properties, as resultants extensively applications such as photocatalysis, sensors, light-emitting diodes, solar cells and electronic transistors (Theerthagiri et al., 2019; AlSalhi et al., 2019). Compared with TiO_2, ZnO as a potential photocatalyst has the advantage of lower cost, absorbing more light quanta and higher photocatalytic efficiency for the degradation of several organic pollutants and removal of bacterial (Di Paola et al., 2012). In particular, ZnO nano flowers efficiently control the bacterial proliferation under UV-light reported by earlier (Talebian et al., 2013; Sirelkhatim et al., 2015). Recently, well-defined ZnO nano/micro-flower particles were prepared by different methods such as hydrothermal, electrochemical, sonochemical, wet chemical (Liu et al., 2006; Li et al., 2008; Xu et al., 2009; Huang et al., 2010; Xie et al., 2011; Chakraborty et al., 2012; Khorsand Zak et al., 2013; Micheal et al., 2020). The hydrothermal technique is a convenience for the crystal growth of ZnO nanostructures (Xie et al., 2011; Sun et al., 2012; Ibupoto et al., 2013). Further, flower particle morphology was transformed into spherically shaped by adding organic surfactants (Zhang et al., 2005; Yuan et al., 2012; Miao et al.,

* Corresponding authors at: Research Chair in Laser Diagnosis of Cancers, Department of Physics and Astronomy, College of Science, King Saud University, Riyadh, Saudi Arabia.
E-mail addresses: malsalhi@ksu.edu.sa (M.S. AlSalhi), rajasekargood@gmail.com (A. Rajasekar).
Peer review under responsibility of King Saud University.

Production and hosting by Elsevier

https://doi.org/10.1016/j.sjbs.2020.02.005
1319-562X/

2016). However, the shapes and size of ZnO crystal are variable and well depend upon the decomposition kinetics of the $Zn(OH)_4^{2+}$ species by the effect of temperature, pH of the medium and reaction time (Zhang et al., 2002; Nicholas et al., 2012). It is considered that the interaction among $Zn(OH)_4^{2-}$coexisting ion cations derived from the hydroxide (NaOH, KOH) affected the ZnO crystal growth process explained by the previous investigators (Uekawa et al., 2004; Sui et al., 2013). Therefore, ammonium hydroxide was utilized in the synthesis of ZnO nanostructure with high crystalline by mild hydrothermal method and tuning of particle morphology by pH of the medium (Zhang et al., 2002; Nicholas et al., 2012). ZnO NPs morphology was synthesized using urease as a nanoreactor at low temperature, from the precursor of zinc nitrate (De La Rica and Matsui, 2008). However, there have been a few reports that have focused on the biologically prepared nanomaterials for various applications (Mandal et al., 2006; Mohanpuria et al., 2008; Narenkumar et al., 2018). To the best of our knowledge, this is the first attempt made in the synthesis of ZnO micro flower structure via thermal shock treatment using ice-cube of zinc ammonium complex on the boiling water surface with the short timing. The structure of ZnO micro flower was tuned by tri-sodium citrate to achieve spherical shape with uniform particle sizes, and UV–Visible spectra calculated bandgap values. By experiments, mechanisms on the synthesis of various ZnO microstructures were proposed. Moreover, the photoinactivation property of these ZnO microstructures (solution suspended particles/coated with glass slide) on *E. coli* cells in an aqueous solution under sunlight was investigated.

2. Materials and methods

2.1. Materials

Zinc acetate (99% pure), 5,5-Dimethyl-1-pyrroline N-oxide (DMPO), silicon wafer and Quartz plate were purchased from Sigma - Aldrich, 40% Urea, Nutrient Broth, Nutrient agar medium, tri-sodium citrate, hexamine and glutaraldehyde solution supplied by Hi-Media, India was used in this study.

2.2. Preparation of biologically activated ammonia from synthetic urine

Ureolytic bacterium of *Bacillus subtilis* (HM475276) was isolated from a railway track environment and identified with molecular techniques as reported by Maruthamuthu et al., 2011. This bacterial strain was used for the production of ammonia from urea broth with the optimum condition and correlated with rail corrosion. In the present study, the synthetic urine was used in the production of ammonia by implement of *Bacillus subtilis* as a bio-catalyst. The composition of synthetic urine (g/l) is as follows: calcium chloride −0.651, magnesium chloride-0.651, potassium chloride-1.6, sodium chloride-4.6, sodium sulfate-2.3, ammonium chloride-1.0, creatinine-1.1, tryptone-10, potassium phosphate-2.8, and urea 40%. The ureolytic bacterium of *Bacillus subtilis* was inoculated with synthetic urine and kept in a bacterial incubator at the room temperature for 7^{th} days. The production of ammonia concentration from that enrichment of bacterial culture on the synthetic urine medium was estimated by the indo-phenol blue method with respect to various time intervals (Dhandapani et al., 2014). Further, the selected bacterial strain (*Bacillus subtilis*) was inoculated into the 250 ml of synthetic urine in a closed container. In this process, two holes were drilled on the top of the box to allow the entry of $O_{2(g)}$ into the container. The presence of $O_{2(g)}$ carried the ammonia$_{(g)}$ from enriched bacterial culture releases into the water, possibly producing ammonium hydroxide.

2.3. Synthesis of ZnO micro-flower particles by thermal shock treatment

The ice-cube of zinc ammonium complex was prepared by base material of zinc acetate and biologically activated ammonia. In a typical procedure, 10.0 g of zinc acetate was dissolved in a 100 ml of millQ water and then biologically activated ammonia was purged into the medium. The medium was transferred into an ice-cube tray and kept for 6 hr on −20 °C to obtain an ice-cube of zinc ammonium complex. Two ice- cubes were added in boiling water surface to form a milky suspension, and then the white colour precipitate was noticed at the bottom of beaker after 15 min. This precipitate was separated from the medium using centrifugation at 6000 rpm for 10 min and then rinsed with distilled water. Further, we have made three thermal profiles (increasing temperature from 35 to 95 °C (T_1, 35 → 95 °C); maintaining of temperature about 95 °C (T_2, >95 °C); and reduction of temperature from 95 to 52 °C (T_3, 95 → 52 °C)) of the medium for making different crystal growth of ZnO microstructures. ZnO particle morphology was tuned by the addition of tri-sodium citrate (0.1 mM) and hexamine (0.1 mM) in zinc ammonium complex to obtain the precipitates noted as ZnO-SC, and ZnO-H system with respectively. The yield calculation of ZnO particles (%) was carried out by the formula:

$$\textit{Weight of the final precipitate Yield of ZnO particles}\ (\%) = \frac{\textit{Weight of the zinc acetate precursors}}{\textit{Weight of the zinc acetate precursors}} \times 100 \quad (1)$$

2.4. Characterization of precipitate materials

The crystal phase of the precipitation samples was analyzed by the PAN analytical advanced Bragg-Brentano X-ray powder diffractometer (XRD) at room temperature over the 2θ range of 10–80° at a step size 0.02 and with a scanning speed of 5°/min (Bruker- D8 ADVANCE). Identification of diffraction peaks was made with software (PANalytical X'Pert High Score). The surface morphology of ZnO particles was observed by FE-SEM, Carl Zeiss SUPRA 55 VP at 30 kV. A Spectra 50 ANALYTIKJENA spectrophotometer was used for recording the UV–Visible spectra of ZnO precipitate samples across the range from 200 to 800 nm. EPR spectroscopy was used to analyze the generation of ·OH radicals in the ZnO particle suspensions medium with the presence of 0.02 mol/L DMPO under the sunlight.

2.5. Sunlight-driven antibacterial activity

Escherichia coli (*E. coli*) cells were cultured in a nutrient broth (Hi-media, Mumbai) and incubated aerobically at 37 °C for overnight. In the present study, photocatalytic inactivation of the ZnO materials was evaluated using *E. coli* cells under sunlight at Karaikudi (10.07 °N-78.80 °E), Tamil Nadu, India. The natural sunlight intensity was measured by Lux meter at regular time intervals and plotted figure given in the Fig. S1. The two experimental conditions were as follows: (i) ZnO particle (0.5 mg) was suspended with 10 ml of phosphate buffer (pH 7.0) in the presence of *E. coli* cells at $\times 10^4$ (CFU/ml). (ii) Photocatalyst material was applied and overcoated (0.4 mg/cm^2 ± 0.02) with glass plate by doctor blade techniques, and the material surface was sterilized by UV-light exposure at 5 min. The interface between the ZnO particles coated the surface and bacterial species by sunlight-driven photocatalytic experiment setup (Fig. S2) was made. The setup configuration is as follow: Quartz plate (5 × 5 × 0.2 cm^2), was placed at bottom, silicon rubber was used to fabricate of 3 × 3 × 0.3 cm^2 cavity for the photocatalytic medium (ZnO particles and *E. coli* cells)

and *E. coli* cells ($\times 10^4$ CFU/ml) suspended in phosphate buffer. Top-side quartz plate (5 × 5 × 0.2 cm^2) contains 1 mm drill for test sample collection (100 µl). Further, various concentrations of *E. coli* cells like $\times 10^2$, $\times 10^4$, $\times 10^6$ (CFU/ml) were used to find photoinactivation using ZnO coated. The photocatalytic medium was exposed to sunlight for 60 min. Tested sample was collected at different time intervals for the enumeration of bacterial cells by pour plate techniques using nutrient agar plate. Reduction of bacterial colonies was calculated from the total viable bacterial counts method. The percentage reduction in bacterial survival rate was calculated using the following formula (Firoz Babu et al., 2012).

$$\text{Bacterial survival rate}\,(\%) = \frac{\text{Viable count}\,(0\,min) - \text{Viable count}\,(\text{time intervals})}{\text{Viable count}\,(0\,min)} \times 100 \qquad (2)$$

A similar approach was followed for the dark condition (control system). All the above experiments were repeated three times, and the average values are presented. Further, the EPR study was carried out to examine the generation of ·OH radicals from the photocatalyst.

2.6. AFM observation of bacterial morphology

AFM (Model Pico scan 2100; (Molecular Imaging, USA) study was conducted to find the bacterial cell morphologies while doing the photocatalytic effect of ZnO particles (before, and after photo treated *E. coli* cells). The bacterial suspension ($\times 10^4$ CFU/ml) with phosphate buffer (pH 7.0) was added to the ZnO particles overcoated with a glass slide and placed in sunlight-driven photocatalytic setup. The bacterial suspension medium was irradiated with sunlight for 20 min. The bacterial sample was harvested by centrifugation at 5,000 rpm for 5 min. The bacterial pellet was resuspended in 2.5% glutaraldehyde solution and kept at 8 °C for 12 hr. The samples were sequentially dehydrated with 20, 40, 60, 80, and 100% ethanol for 10 min. 100 µl samples were dropped into a clean silicon wafer (1 × 1 cm^2), and then gently air-dried to observe the morphology of bacteria. The bacterial morphology was analyzed using gold-coated SiN_3 cantilevers.

3. Result and discussion

Human urine can be utilized for ureolytic bacterial strain to produce the biologically active ammonia via enzyme urease (Maruthamuthu et al., 2011). This bacterial strain is capable of hydrolyzing urea content to ammonia and carbonic acid, which utilize urea as a sole nitrogen source for its growth. In the present study, ureolytic bacterium of *Bacillus subtillis* was used for the production of biogenic ammonia from synthetic urine. Fig. S3 depicts the ammonia concentration of synthetic urine at regular intervals of time in the presence of *Bacillus subtillis* with optimum condition. It can be observed that the ammonia concentration was maximum 22,500 ppm at 6th days. The membrane filters method was used for the removed bacterial species and calcium phosphate or carbonate particles from bacterial enrichment cultures, leaving ammonia behind. Thus formed biologically activated ammonia combines with $CO_{2(g)}$ from bacterial respiration, giving rise to resultant products such as, ammonium carbonate and ammonium bicarbonate, which was utilized for the synthesis of hairy shaped ZnO nanostructures (Dhandapani et al., 2020). Further, collections of ammonia$_{(g)}$ by direct purging of $O_{2(g)}$ method was obtained low concentration of ammonia maximum at 4000 ppm. This method can be suitable for the synthesis of ZnO microstructure, owing to the purify of bio-genic ammonia (non-availability of anions such as chloride, sulfate, carbonate).

3.1. Ice-cube mediated synthesis of ZnO micro flower particles

In a typical experiment, zinc acetate reacted with biologically activated ammonia and formed as zinc ammonium complex at pH 10.5. These complexes were trapped by ice-crystal in the deep freezer for 1hr (Fig. 1a). The thermal shock mediated synthesis of ZnO microstructures on the boiling water are shown in Fig. 1(b-e) at various time intervals. The thermal camera was utilized for capturing the temperature of the medium, which initially displayed above 95 °C around the medium (Fig. 1f). Ice-cubes of zinc ammonium complex was added in boiling water medium and reduction in temperature was observed. It is due to the variation in ice-cube temperature (−4 °C). Ice-cube was thoroughly dispersed in the boiling water within 30 sec. The last generated thermal shock at the interface of ice-cube and boiling water was noticed. A white colour suspension was formed, and the particles were dispersed in the medium (Fig. 1e).

3.2. Structure and morphology

Fig. 2 shows XRD patterns of the precipitated samples. All the diffraction peaks were identified and indexed to the wurtzite hexagonal ZnO (JCPDs No: 89-0510). XRD pattern confirmed the presence of ZnO crystal phase with a little impurity of $Zn(OH)_2$ in the precipitated sample at T_3, 95 → 52 °C. The formation of $Zn(OH)_2$ may be due to the reduction of temperature in this process.

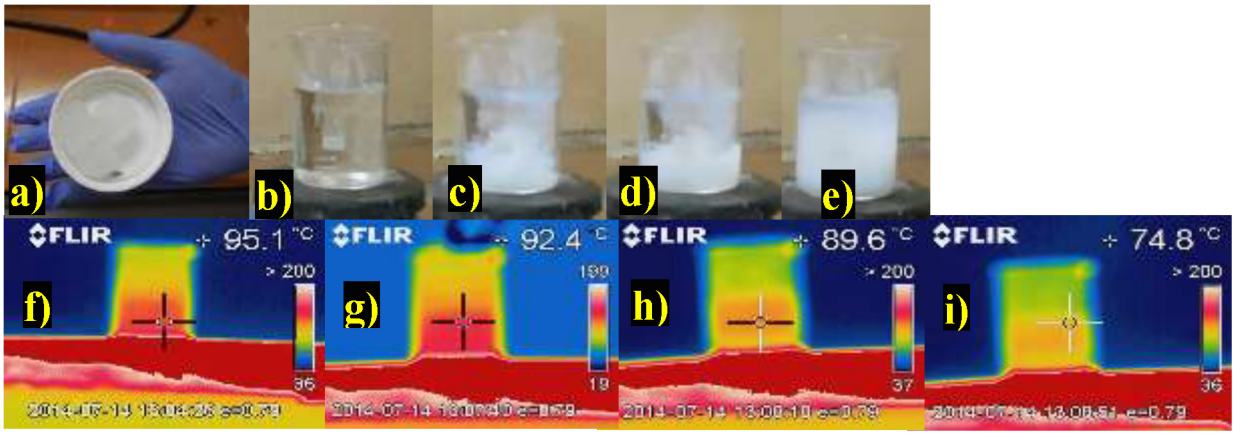

Fig. 1. Visual view of (a) ice-cube of zinc ammonium complex, (b-e) thermal shock mediated synthesis of ZnO microstructures at 1 min and (e-h) thermal camera captured in temperature of the medium.

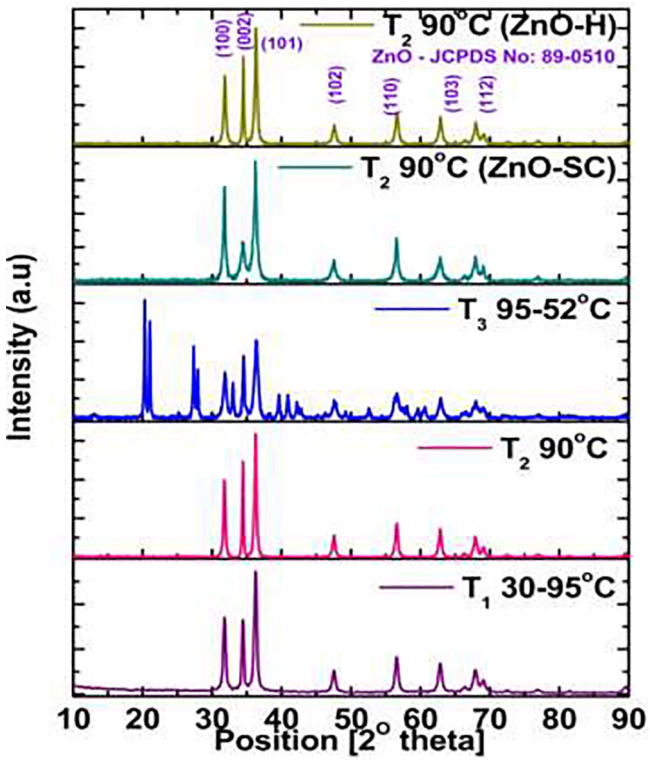

Fig. 2. XRD pattern of the thermal shock mediated synthesis of ZnO microstructures with and without surfactant.

ZnO crystal phase without any impurity was observed in the precipitated samples of T_1, 35 → 95 °C and T_2, >95 °C. Further, we noted two different precipitated samples in ZnO crystal plane (022) from T_2 while adding trisodium citrate and hexamine surfactant into ice-cube precursors. These results indicate that the citrate ion control ZnO crystal phases in zinc ammonium complex during the synthesis, and there were no significant changes noticed in the crystal phase of ZnO-H when compared to ZnO (Fig. 2) while using hexamine. XRD pattern study revealed that the synthesized products have wurtzite hexagonal ZnO crystals structures and modified crystal planes were noticed while adding surfactants.

Fig. 3a shows FE-SEM images of ZnO particle morphologies obtained at T_1, 35 → 95 °C, where non-flower like structure with cluster formation was observed, and particle size distribution was 1.5 to 2.5 μm. At constant temperature (T_2, >95 °C), the morphology of particles was a flower-like structure with a non-uniform particle size distribution between 2 and 4 μm as seen in Fig. 3b. During the decreasing of temperature profile (T_3, 95 → 52 °C), the particle morphology was diamond-shaped with the size of <1 μm as presented in Fig. 3c. It can be concluded that the growth of ZnO particle morphologies depends upon the temperature of the medium.

3.3. Mechanism for the formation of micro flower-shaped ZnO microstructures

Several investigators have reported that hydrothermal method is suitable for preparation of ZnO micro and even nanostructures with a variety of morphologies such as flower, rod, spherical, sponge and diamond through the formation of zinc ammonium

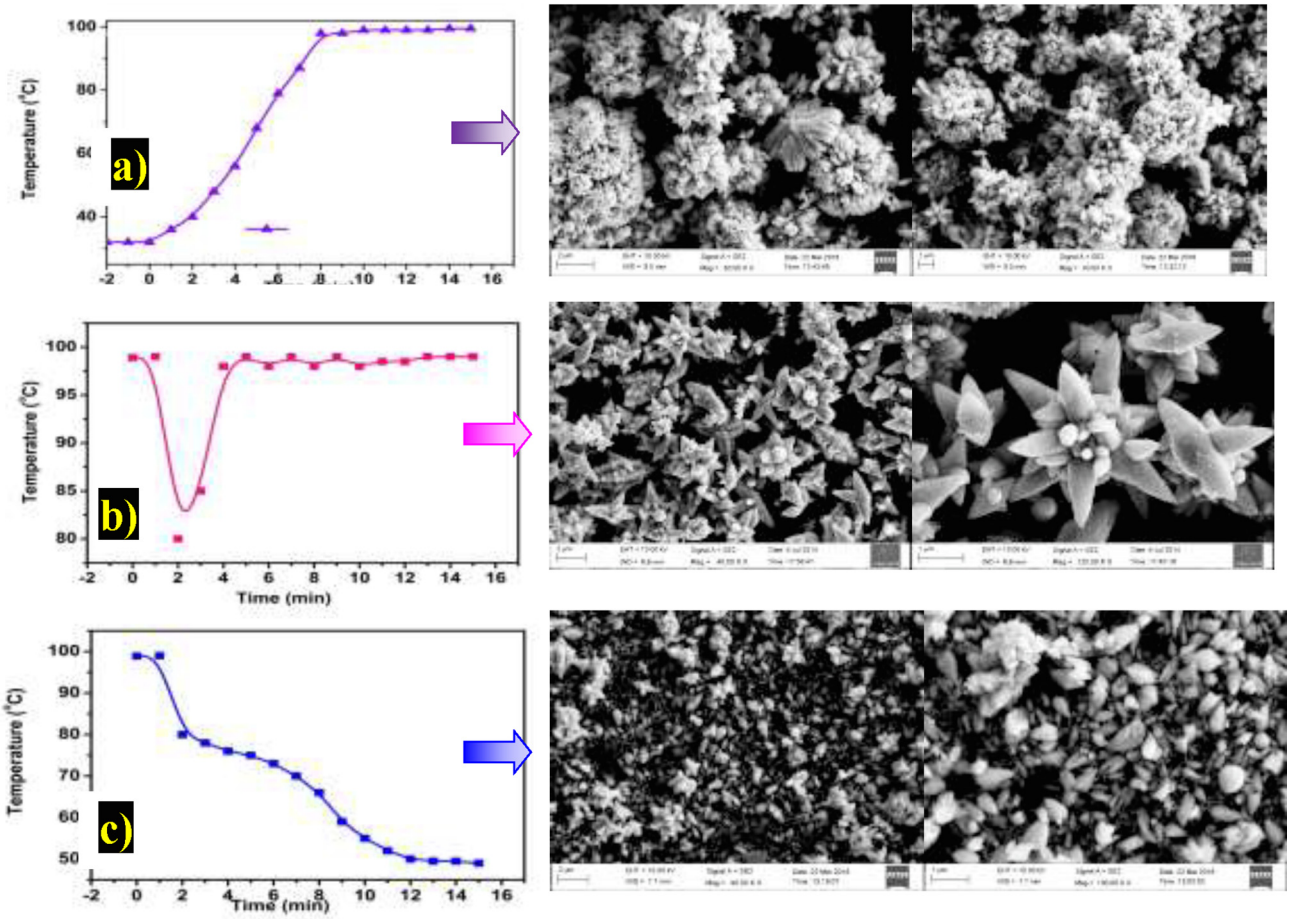

Fig. 3. FE-SEM images of the ZnO microstructures.

complexes as an intermediate (Zhang et al., 2002; Zhang et al., 2004; Zhang et al., 2005; Xie et al., 2011). The overall reaction for the growth of ZnO nanocrystalline is expressed as follows (Zhang et al., 2002).

$$Zn(NH_3)_4^{2+} + 2OH^- \rightarrow ZnO + 4NH_3 + H_2O \quad (1)$$

$$Zn(OH)_4^{2-} \rightarrow ZnO + H_2O + 2OH^- \quad (2)$$

In the present study, the biologically activated ammonia reacts with zinc acetate and forms zinc ammonium complex. The ice-cube crystal was used as entrapped zinc ammonium complex, which controls the release of zinc ammonium complex into boiling water as a resultant ZnO micro flower-like structure (Fig. 4). It can be assumed that the above two possible reactions occurred at the interface between ice-cube and boiling water (Eq. (1) and (2)). However, ice-cube of zinc ammonium complex are spat by thermal shock at boiling water interface to form as $Zn(OH)_4^{2-}$ nuclei or ZnO within a sec. Another possibility is the generation of $Zn(OH)_4^{2-}$ at the interface of ice- cube which travelled to medium and formed as ZnO, here the travelling period was sufficient for the formation of ZnO microstructures.

Further, chemical ammonia was used for the synthesis of ZnO flower. The chemically formed ZnO particle was similar to biomediated ZnO microstructures (Fig. 5). It can also be explained that the addition of surfactants hexamine and trisodium citrate determine the morphology of ZnO particles where flower and sphere (Fig. 6a-b) were noticed respectively. It is due to the interaction between $Zn(OH)_4^{2-}$ nuclei and surfactants (Yuan et al., 2012). The percentage of yield and particle morphologies with particle size distribution was summarized in Table.1. The high yield rate was

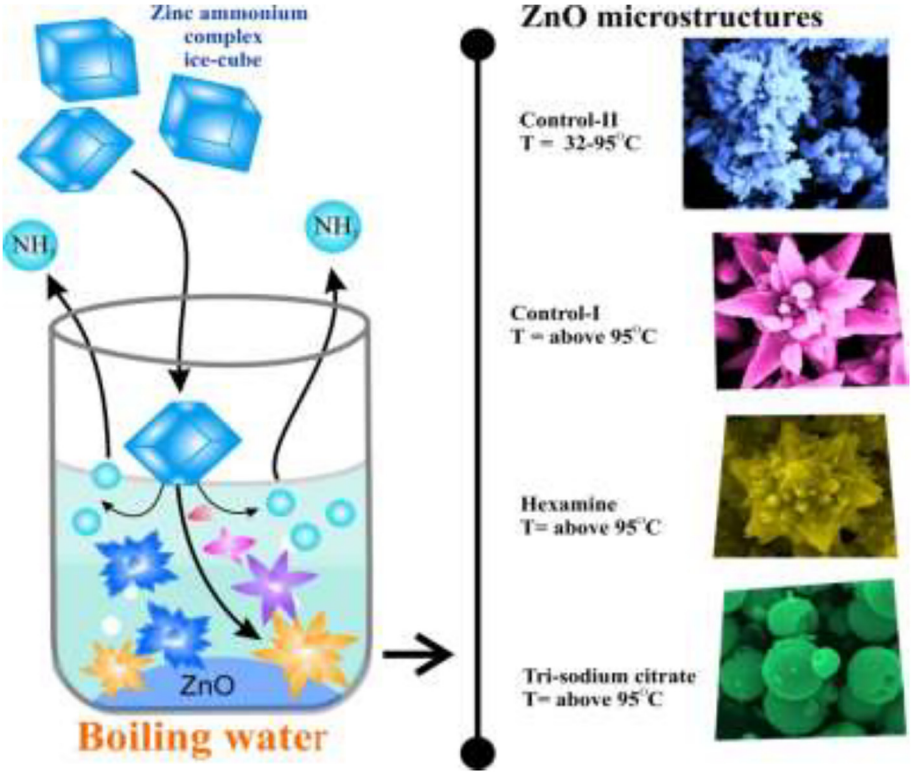

Fig. 4. Schematics representation of the ice-cube mediated synthesis of ZnO microstructures.

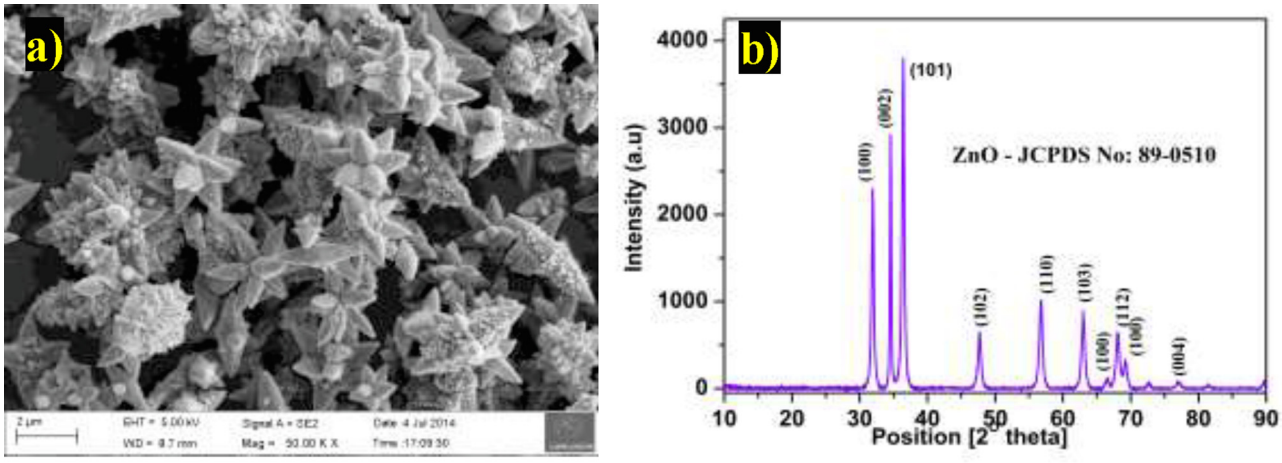

Fig. 5. (a) FE-SEM image and (b) XRD pattern of the ZnO microstructure synthesized by chemical ammonia method.

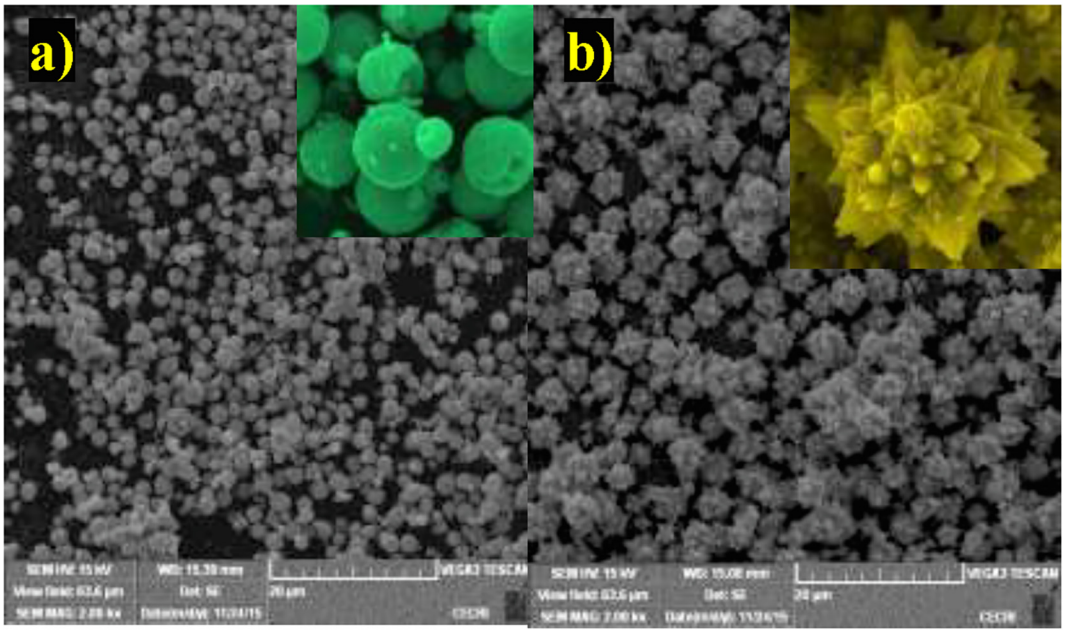

Fig. 6. SEM images of the ZnO micro flower structures tuned with trisodium citrate and hexamine to achieve (a) spherical and (b) flower respectively.

Table 1
Yield percentage of ZnO microstructure by ice-cube mediated synthesis.

S. No	System	Morphology	Size (μm)	Yield (%)
1	T_1, 35 → 95 °C	flower cluster	0.5–1.5	60
2	T_2, >95 °C	flower non-uniform	2–4	89
3	T_3, 95 → 52 °C	paddle	>1	45
4	T_2, >95 °C (ZnO-H)	flower uniform	3–4	85
5	T_2, >95 °C (ZnO-SC)	spherical with uniform	2–2.5	92

attained at 95°C. At low temperature, the presence of ammonia formed as $Zn(OH)_2$ and $Zn(NH_3)_4^{2+}$ complex (Oswald process) which changed the shape of the particles and reduced the yield (Wu et al., 2016).

3.4. UV–Visible spectra

Bandgap values were calculated for the synthesized ZnO particles using UV–Visible spectrum and presented in Fig. S4. ZnO microstructures like particles, flower, flower-H and sphere were found to be bandgap 3.25, 3.20, 3.21 and 3.23 eV respectively. All band gap values are closer to chemically synthesized ZnO particles (Singh et al., 2019). These materials are useful to offer a photocatalytic inactivation of bacterial species under the sunlight.

3.5. EPR study

Lipovsky et al., 2009 demonstrated the formation of hydroxyl radicals in water suspensions of ZnO particles under the illumination of visible light (400–500 nm) by using the DMPO spin trap as ·OH radicals. Fig. S5 shows the EPR spectra for the ice-mediated synthesis of various particles morphology in ZnO under the sunlight and dark conditions. It can be seen that four distinct peaks were obtained from all ZnO samples under the sunlight condition, which can be attributed to the hydroxyl radical generation. The present result was similar to our previous report (Dhandapani et al., 2020). Those peaks were absent in the dark condition. EPR study clearly indicated that hydroxyl radical generation from the ZnO particle surface under the sunlight exposure. There is no significant difference in the EPR spectrum for all ZnO particles.

3.6. Antibacterial activity

In the present study, synthesized ZnO particle with various morphologies was evaluated by sunlight-driven photokilling efficiency using *E. coli* cells ($\times 10^6$ CFU/ml) under sunlight and dark condition. The bacterial survival rate was completely nullified after 15–60 min of light exposure (Fig. 7a). The flower particles showed excellent performance on bacterial killing efficiency when compared to other particles. During the dark condition, the maximum *E. coli* survival rate was 85% (Fig. 7a). This study reveals that the photokilling efficiency of *E. coli* was found to be highly dependent on ZnO particle morphology. ZnO flower showed 0% bacterial survival rate at 15 min. Further, the bacterial killing efficiency under ZnO flower coating was checked using different concentrations of bacteria (*E. coli* bacterial cells at $\times 10^2$, $\times 10^4$ & $\times 10^6$ CFU/ml under the sunlight and dark condition). It was a significant reduction of the bacterial survival rate after 10 min of light exposure in the presence of *E. coli* cells $\times$ 10^2 CFU/ml (Fig. 7b). The bacterial survival rate was 10% and 40% while using $\times 10^4$, $\times 10^6$ CFU/ml of *E. coli* cells respectively. There was a weak DMPO-·OH signal noticed in the usage of bacterial test solution of $\times$ 10^4, x 10^6 CFU/ml, when compared to *E. coli* cells of $\times 10^2$ CFU/ml (Fig. 8a). The increased bacterial concentrations may interfere with light penetration on ZnO photocatalyst active material surface which reduced the concentration of ·OH radical generation (Fig. 8b). Lam et al., 2017 reported that surfactant-free synthesis of ZnO micro/nanoflowers with efficient photocatalytic antibacterial performance against *E. coli*. ZnO nanorods were utilized to study their sunlight-induced bactericidal activity against *S. aureus* (Singh et al., 2019). Ag/Fe_2O_3/ZnO heterostructure promoted faster *E. coli*

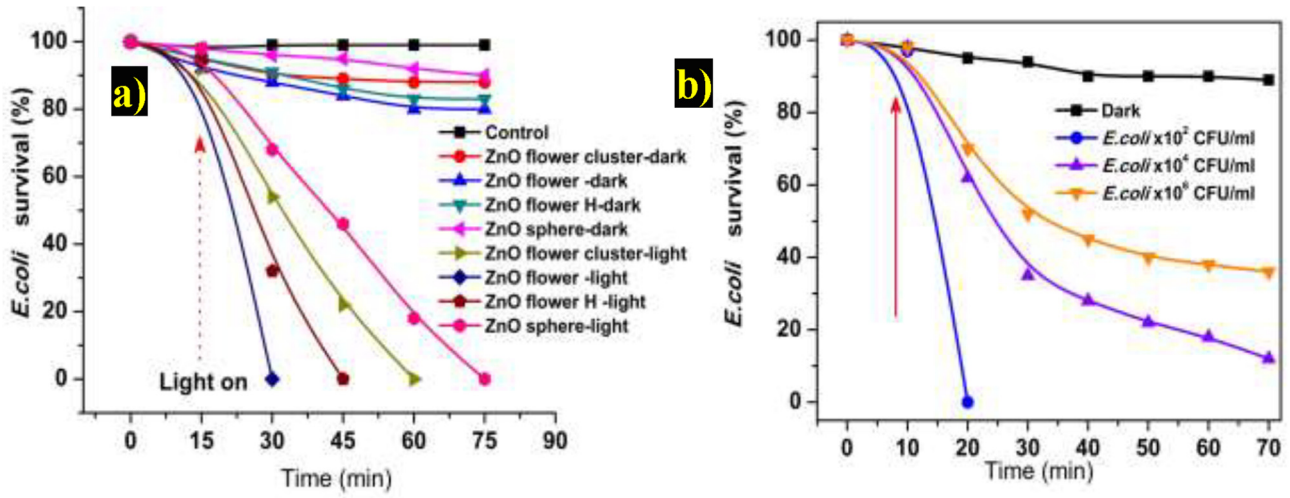

Fig. 7. (a) For comparison the results of percentage survival of *E. coli* vs. sunlight irradiation time for the inactivation of bacteria using various ZnO microstructures at solution suspension condition and (b) ZnO micro flower overcoated with a glass slide.

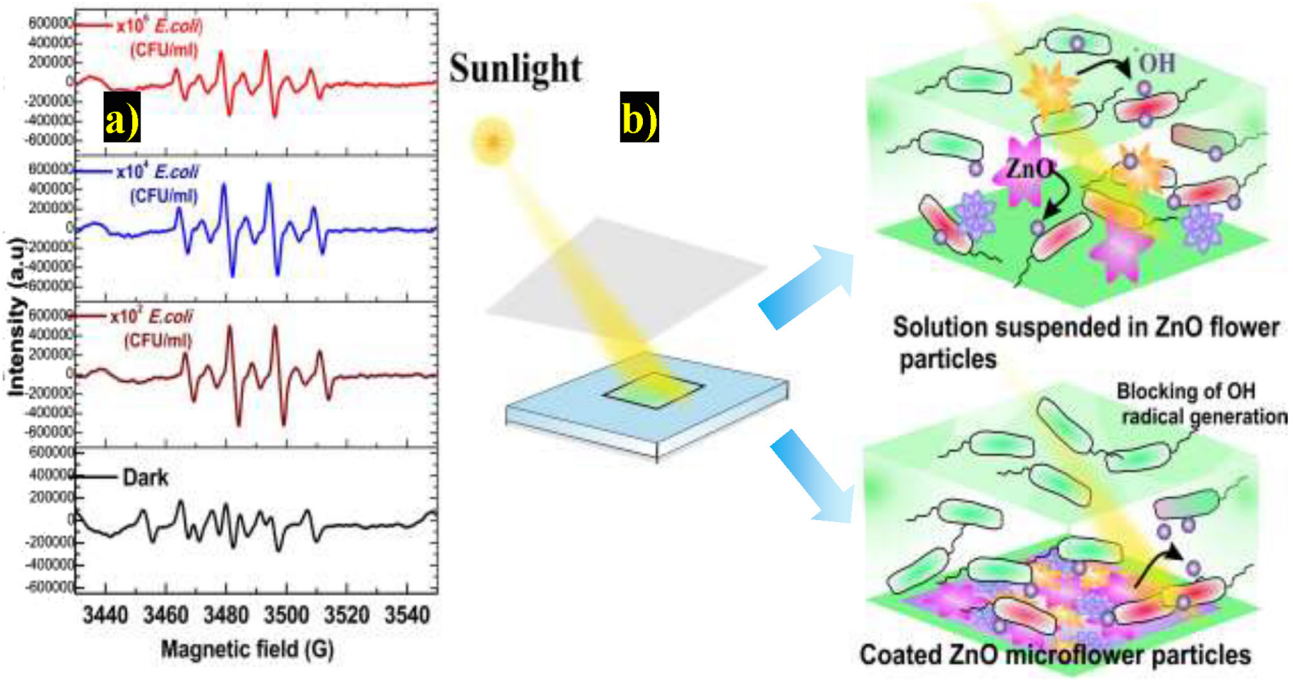

Fig. 8. (a) EPR spectra of ·OH radical trapped by DMPO in ZnO micro flower particle with the bacterial test medium at 20 min sunlight exposure and (b) schematic representation of the photoinactivation of *E. coli* cells on the solution suspension and ZnO microstructures overcoated with a glass slide.

deactivation under visible light as compared to a dark environment. The generation of reactive oxygen species (ROS) species appears to be a key factor in the enhanced activity under visible light (Kaur et al., 2019). *A. baumannii* and *K. pneumonia* were significantly eradicated by the 0.1 mg/mL ZnO NPs with 10.8 J/cm^2 of blue light with the optimum condition (Yang et al., 2018). A new approach of applying combined ultrasonication and light irradiation to ZnO NPs has been attempted to enhance their antibacterial activity against *E. coli* (Zhang et al., 2017). The prepared ZnO microstructures material revealed an efficient sunlight photo inactivation of *E. coli* when compared to dark condition. The present result was made by previous investigators (Zhang et al., 2017; Kaur et al., 2019; Lam et al., 2017).

3.7. Bacterial cell morphology observation

The bacterial cell morphology (before and after photo treated *E. coli* cells) was observed by AFM. Untreated *E. coli* cells were 1.0–3.2 μm long rods with a smooth surface (Fig. 9a). The sunlight irradiation on the ZnO coated material ruptured the *E. coli* cells ($\times 10^6$ CFU/ml) and collapsed the structure of the cell presented in Fig. 9b. Based on the results are propose mechanisms for photoinactivation of *E. coli* by ZnO microstructures under sunlight exposure. ZnO is a wide band-gap semiconductor and consequently undergoes photo excitation by sunlight. The photo excitation of ZnO particle was initiates electron transfer from the valence band to the conduction band, thus creating an electron-hole pair. The

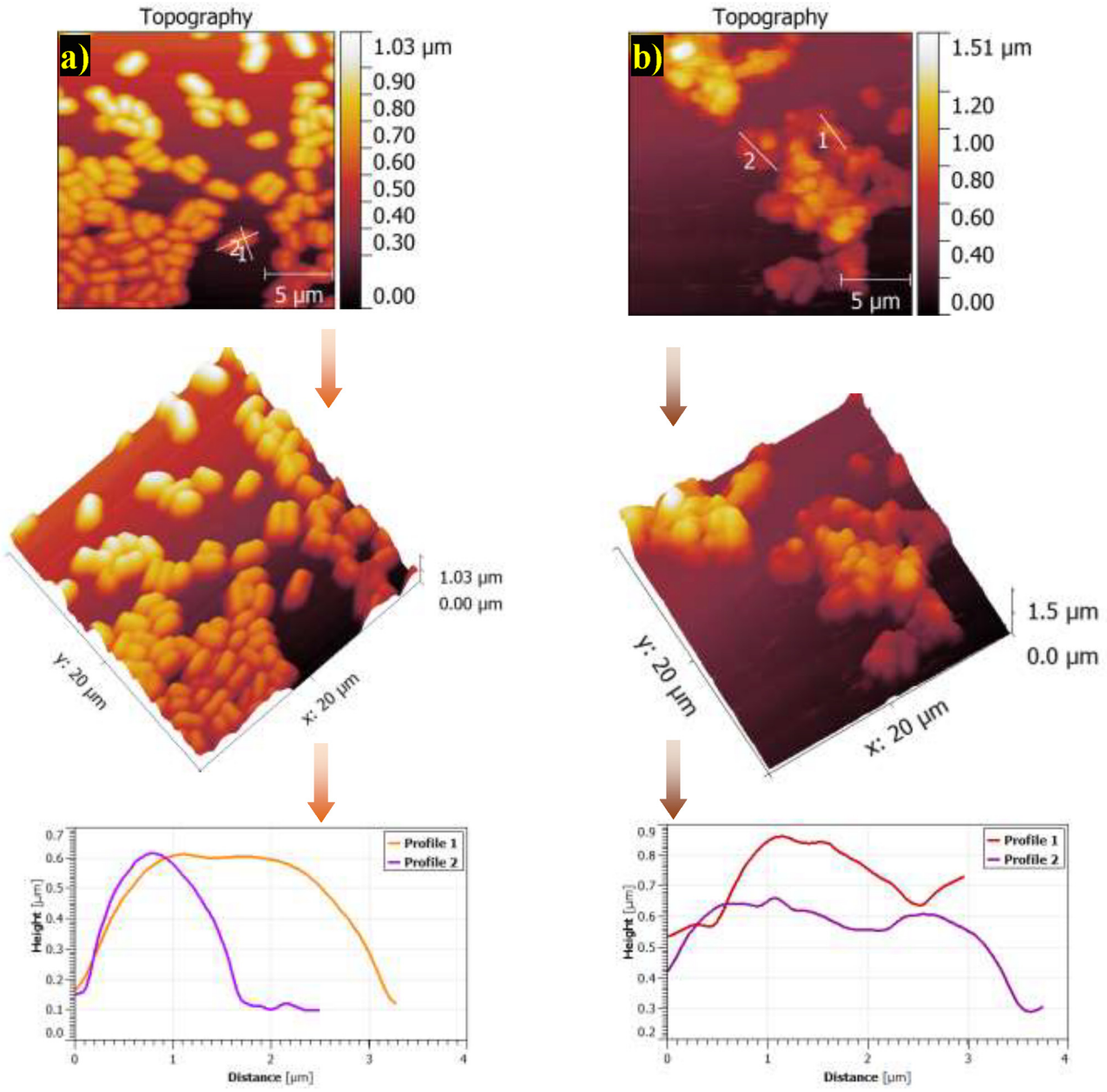

Fig. 9. AFM images with profile parameters (a) before and (b) after photo treated *E. coli* cells on the ZnO microstructures overcoated with a glass slide.

photo-induced electrons and holes can induce a series of photochemical reactions to generate ·OH radicals at the NP surface in an aqueous suspension (Zhang et al., 2017). This postulation was confirmed from our EPR studies. The photocatalytic generation of ·OH radicals under the influence of sunlight killed the nearby bacterial cells (Ying et al., 2005; Sapkota et al., 2011). The present study could serve as an efficient strategy for biomedical application.

4. Conclusions

ZnO particles with various morphologies were successfully synthesized by the ice-cube method at short timing duration. The temperature of the medium had a significant role in the synthesis of ZnO particulate matter and confirmed by FE-SEM and XRD pattern. Trisodium citrate tuned the morphology of ZnO flower to sphere particles. The sunlight-driven photocatalytic experiment showed the excellent performance of the antibacterial activity of ZnO particles against *E. coli* bacterium cells. The photoinactivation of *E. coli* was found to be highly dependent on the ZnO particle morphology. When increasing the bacterial concentrations, light penetration was reduced due to the attachment of bacteria to ZnO particles which blocks the ·OH radical generation. AFM study confirmed the bacterial cell membrane destruction by the photocatalytic activity of ZnO flower particles.

Declaration of Competing Interest

The authors declare that they have no known competing financial interests or personal relationships that could have appeared to influence the work reported in this paper.

Acknowledgement

The authors are grateful to the Deanship of Scientific Research, King Saud University for funding through Vice Deanship of Scientific Research Chairs.

Appendix A. Supplementary material

Supplementary data to this article can be found online at https://doi.org/10.1016/j.sjbs.2020.02.005.

References

AlSalhi, M.S., Sakthisabarimoorthi, A., Devanesan, S., Martin Britto Dhas, S.A., Jose, M., 2019. Study on photocatalytic and impedance spectroscopy investigations of composite CuO/ZnO nanoparticles. J. Mater. Sci.: Mater. Electron. 30, 13708–13718.

Chakraborty, S., Kole, A.K., Kumbhakar, P., 2012. Room temperature chemical synthesis of flower-like ZnO nanostructures. Mater. Lett. 67, 362–364.

De La Rica, R., Matsui, H., 2008. Urease as a nanoreactor for growing crystalline ZnO nanoshells at room temperature. Angew. Chemie - Int. Ed. 47, 5415–5417.

Dhandapani, P., Prakash, A.A., AlSalhi, M.S., Maruthamuthu, S., Devanesan, S., Rajasekar, A., 2020. Ureolytic bacteria mediated synthesis of hairy ZnO nanostructure as photocatalyst for decolorization of dyes. Mater. Chem. Phys. 122619

Dhandapani, P., Siddarth, A.S., Kamalasekaran, S., Maruthamuthu, S., Rajagopal, G., 2014. Bio-approach: ureolytic bacteria mediated synthesis of ZnO nanocrystals on cotton fabric and evaluation of their antibacterial properties. Carbohydr. Polym. 103, 448–455.

Di Paola, A., García-López, E., Marcì, G., Palmisano, L., 2012. A survey of photocatalytic materials for environmental remediation. J. Hazard. Mater. 211, 3–29.

Firoz Babu, K., Dhandapani, P., Maruthamuthu, S., Anbu Kulandainathan, M., 2012. One pot synthesis of polypyrrole silver nanocomposite on cotton fabrics for multifunctional property. Carbohydr. Polym. 90, 1557–1563.

Huang, J., Wu, Y., Gu, C., Zhai, M., Yu, K., Yang, M., Liu, J., 2010. Large-scale synthesis of flowerlike ZnO nanostructure by a simple chemical solution route and its gas-sensing property. Sens. Actuators, B Chem. 146, 206–212.

Ibupoto, Z., Khun, K., Eriksson, M., AlSalhi, M.S., Atif, M., Ansari, A., Willander, M., 2013. Hydrothermal growth of vertically aligned ZnO nanorods using a biocomposite seed layer of ZnO nanoparticles. Materials 6, 3584–3597.

Kaur, A., Anderson, W.A., Tanvir, S., Kansal, S.K., 2019. Solar light active silver/iron oxide/zinc oxide heterostructure for photodegradation of ciprofloxacin, transformation products and antibacterial activity. J. Colloid Interface Sci. 557, 236–253.

Khorsand Zak, A., Majid, W.H.A., Wang, H.Z., Yousefi, R., Moradi Golsheikh, A., Ren, Z. F., 2013. Sonochemical synthesis of hierarchical ZnO nanostructures. Ultrason. Sonochem. 20, 395–400.

Lam, S.M., Quek, J.A., Sin, J.C., 2017. Surfactant-free synthesis of ZnO micro/nanoflowers with efficient photocatalytic antibacterial performance. Mater. Lett. 195, 34–36.

Li, Z., Huang, X., Liu, J., Li, Y., Li, G., 2008. Morphology control and transition of ZnO nanorod arrays by a simple hydrothermal method. Mater. Lett. 62, 1503–1506.

Lipovsky, A., Tzitrinovich, Z., Friedmann, H., Applerot, G., Gedanken, A., Lubart, R., 2009. EPR study of visible light-induced ROS generation by nanoparticles of ZnO. J. Phys. Chem. C 113, 15997–16001.

Liu, J., Huang, X., Li, Y., Duan, J., Ai, H., 2006. Large-scale synthesis of flower-like ZnO structures by a surfactant-free and low-temperature process. Mater. Chem. Phys. 98, 523–527.

Mandal, D., Bolander, M.E., Mukhopadhyay, D., Sarkar, G., Mukherjee, P., 2006. The use of microorganisms for the formation of metal nanoparticles and their application. Appl. Microbiol. Biotechnol. 69, 485–492.

Maruthamuthu, S., Nagendran, T., Anandkumar, B., Karthikeyan, M.S., Palaniswamy, N., Narayanan, G., 2011. Microbiologically influenced corrosion on rails. Curr. Sci. 100, 870–880.

Miao, Y., Zhang, H., Yuan, S., Jiao, Z., Zhu, X., 2016. Preparation of flower-like ZnO architectures assembled with nanosheets for enhanced photocatalytic activity. J. Colloid Interface Sci. 462, 9–18.

Micheal, K., Ayeshamariam, A., Devanesan, S., Bhuvaneswari, K., Pazhanivel, T., AlSalhi, M.S., Aljaafreh, M.J., 2020. Environmental friendly synthesis of carbon nanoplates supported ZnO nanorods for enhanced degradation of dyes and organic pollutants with visible light driven photocatalytic performance. J. King Saud Univ. – Sci. 32, 1081–1087.

Mohanpuria, P., Rana, N.K., Yadav, S.K., 2008. Biosynthesis of nanoparticles: technological concepts and future applications. J. Nanoparticle Res 10, 507–517.

Narenkumar, J., Parthipan, P., Madhavan, J., Murugan, K., Marpu, S.B., Suresh, A.K., Rajasekar, A., 2018. Bioengineered silver nanoparticles as potent anti-corrosive inhibitor for mild steel in cooling towers. Environ. Sci. Pollut. Res. 25, 5412–5420.

Nicholas, N.J., Franks, G.V., Ducker, W.A., 2012. The mechanism for hydrothermal growth of zinc oxide. Cryst. Eng. Comm. 14, 1232–1240.

Sapkota, A., Anceno, A.J., Baruah, S., Shipin, O.V., 2011. Zinc oxide nanorod mediated visible light photoinactivation of model microbes in water. Nanotechnology 22, 215703.

Singh, J., Juneja, S., Palsaniya, S., Manna, A.K., Soni, R.K., Bhattacharya, J., 2019. Evidence of oxygen defects mediated enhanced photocatalytic and antibacterial performance of ZnO nanorods. Colloids Surf. B 184, 110541.

Sirelkhatim, A., Mahmud, S., Seeni, A., Kaus, N.H.M., Ann, L.C., Bakhori, S.K,M., Hasan, H., Mohamad. D., 2015. Review on zinc oxide nanoparticles: antibacterial activity and toxicity mechanism. Nano-Micro Lett. 7, 219–242.

Sui, M., Zhang, L., Sheng, L., Huang, S., She, L., 2013. Synthesis of ZnO coated multi-walled carbon nanotubes and their antibacterial activities. Sci. Total Environ. 452, 148–154.

Sun, L., Shao, R., Chen, Z., Tang, L., Dai, Y., 2012. Ding. Alkali-dependent synthesis of flower-like ZnO structures with enhanced photocatalytic activity via a facile hydrothermal method. J. Appl. Surf. Sci. 258, 5455–5461.

Talebian, N., Amininezhad, S.M., Doudi, M., 2013. Controllable synthesis of ZnO nanoparticles and their morphology-dependent antibacterial and optical properties. J. Photochem. Photobiol. B Biol. 120, 66–73.

Theerthagiri, J., Salla, S., Senthil, R.A., Nithyadharseni, P., Madankumar, A., Arunachalam, P., Maiyalagan, T., Kim, H.S., 2019. A review on ZnO nanostructured materials: energy, environmental and biological applications. Nanotechnology 30, 392001.

Uekawa, N., Yamashita, R., Jun, Y., Wu, Kakegawa, W., 2004. Effect of alkali metal hydroxide on formation processes of zinc oxide crystallites from aqueous solutions containing $Zn(OH)_4^{2-}$ ions. Phys. Chem. Chem. Phys. 6, 442–446.

Wu, Z., Yang, S., Wu, W., 2016. Shape control of inorganic nanoparticles from solution. Nanoscale 8, 1237–1259.

Xie, J., Wang, H., Duan, M., Zhang, L., 2011. Synthesis and photocatalysis properties of ZnO structures with different morphologies via hydrothermal method. Appl. Surf. Sci. 257, 6358–6363.

Xu, L., Hu, Y.L., Pelligra, C., Chen, C.H., Jin, L., Huang, H., Sithambaram, S., Aindow, M., Joesten, R., Suib, S.L., 2009. ZnO with different morphologies synthesized by solvothermal methods for enhanced photocatalytic activity. Chem. Mater. 21, 2875–2885.

Yang, M.Y., Chang, K.C., Chen, L.Y., Wang, P.C., Chou, C.C., Wu, Z.B., Hu, A., 2018. Blue light irradiation triggers the antimicrobial potential of ZnO nanoparticles on drug-resistant Acinetobacter baumannii. J. Photochem. Photobiol., B 180, 235–242.

Ying, W., Xudong, Y., Yunqiu, W., Yongbao, W., Zhiyong, H., 2005. Disinfection and bactericidal effect using photocatalytic oxidation. HKIE Trans. 12, 39–43.

Yuan, G., Zhu, J., Li, C., Gao, X., 2012. Morphology-controllable electrochemical synthesis and photoluminescence properties of ZnO nanocrystals with porous structures. Cryst. Eng. Comm. 14, 7450.

Zhang, H., Yang, D., Li, D., Ma, X., Li, S., Que, D., 2005. Controllable growth of ZnO microcrystals by a capping-molecule-assisted hydrothermal process. Cryst. Growth Des. 5, 547–550.

Zhang, H., Yang, D., Ma, X., Ji, Y., Xu, J., Que, D., 2004. Synthesis of flower-like ZnO nanostructures by an organic-free hydrothermal process. Nanotechnology 15, 622–626.

Zhang, J., Sun, L., Yin, J., Su, H., Liao, C., Yan, C., 2002. Control of ZnO morphology via a simple solution route. Chem. Mater. 14, 4172–4177.

Zhang, L., Qi, H., Yan, Z., Gu, Y., Sun, W., Zewde, A.A., 2017. Sonophotocatalytic inactivation of *E. coli* using ZnO nanofluids and its mechanism. Ultrason. Sonochem. 34, 232–238.

Zhou, B., Shi, B., Jin, D., Liu, X., 2015. Controlling upconversion nanocrystals for emerging applications. Nat. Nanotechnol. 10, 924–936.